Scaling Theory for Unipolar Resistance Switching

J. S. Lee,[1] S. B. Lee,[1] S. H. Chang,[1] L. G. Gao,[1] B. S. Kang,[2] M.-J. Lee,[3] C. J. Kim,[3] T. W. Noh,[1,*] and B. Kahng[1,4,†]

[1]*Department of Physics and Astronomy, Seoul National University, Seoul 151-747, Korea*
[2]*Department of Applied Physics, Hanyang University, Ansan, Gyeonggi-do 426-791, Republic of Korea*
[3]*Samsung Advanced Institute of Technology, Yongin 440-600, Republic of Korea*
[4]*School of Physics, Korea Institute for Advanced Study, Seoul 130-722, Republic of Korea*

(Received 19 June 2010; revised manuscript received 4 October 2010; published 9 November 2010)

We investigate a reversible percolation system showing unipolar resistance switching in which percolating paths are created and broken alternately by the application of an electric bias. Owing to the dynamical changes in the percolating paths, different from those in classical percolating paths, a detailed understanding of the structure is demanding and challenging. Here, we develop a scaling theory that can explain the transport properties of these conducting paths; the theory is based on the fractal geometry of a percolating cluster. This theory predicts that two scaling behaviors emerge, depending on the topologies of the conducting paths. We confirm these theoretical predictions experimentally by observing material-independent universal scaling behaviors in unipolar resistance switching.

DOI: 10.1103/PhysRevLett.105.205701 PACS numbers: 05.60.Cd, 05.45.Df, 64.60.ah, 72.20.−i

During the dielectric breakdown of an insulating medium, conducting paths with a fractal pattern are instantaneously formed [1–4]. Interestingly, in numerous thin insulating media positioned between top and bottom electrodes, as shown in Fig. 1(a), a well-controlled dielectric breakdown can lead to the formation of nanoscale conducting paths or filaments [5–11]. These paths can be ruptured and reconnected alternately through a dielectric breakdown [11] and the thermal fuse effect [9,12–14], respectively, by successively applying an electric bias. This nonvolatile resistance change, called unipolar resistance switching, has potential importance for next-generation memory devices.

To explain the switching dynamics, a dynamic bond-percolation model, called the random circuit breaker (RCB) network model [8,12], has been introduced. In this model, an initial insulating configuration is mostly composed of off-state (insulating) bonds, with a few on-state (conducting) bonds, as shown in Fig. 1(b). Conducting paths are then created [Fig. 1(c)] via a dielectric breakdown; off → on switching occurs when the applied voltage of an off-state bond is larger than some threshold V_c, as in Fig. 1(d). These percolating paths can break via the thermal fuse effect triggered by Joule heating. When the temperature of on-state bonds exceeds some threshold T_c, the hottest (on-state) bonds located in the bottleneck of the entire paths are burnt and transformed into off-state bonds, as shown in Fig. 1(e), which results in the rupturing of paths [Fig. 1(f)].

While numerical results based on this RCB model have been successful in explaining experimental results qualitatively [8,12], the scaling relations [15] observed experimentally for a single material NiO between the resistance, the third harmonic generation signal, and the rupture current have not been explained yet. It is manifest that such physical quantities depend on topological features of percolating paths created through alternating dielectric breakdown and rupture processes, which are different from those of the classical percolation model created through random processes. Nevertheless, the topology of the percolating paths in the RCB model has not been studied yet. In this Letter, first we study structural properties of the percolating paths, and then develop a scaling theory, which successfully explains the scaling relations experimentally

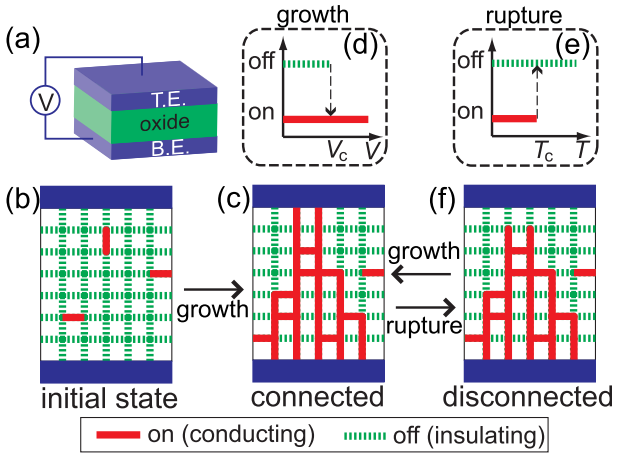

FIG. 1 (color online). (a) Schematic of an electrode-oxide-electrode structure. (b) Initial configuration of an insulating medium with a few on-state bonds as defects. (c) Snapshot of percolating (highly conducting) paths created via the dielectric breakdown process. (d) The off → on switching by a dielectric breakdown, which occurs when the applied voltage exceeds some threshold voltage V_c. (e) The on → off switching by the thermal fuse effect, which occurs when the temperature of a bond exceeds some threshold temperature T_c because of Joule heating. (f) Snapshot of disconnected paths ruptured by the thermal fuse effect.

observed. Finally, we conduct the unipolar resistance switching experiments for several different materials, and confirm universal scaling behaviors.

Let us first investigate the topological feature of the paths. It has been found theoretically and experimentally that the structure of conducting paths created via this dielectric breakdown process is different from simple integer-dimensional shapes such as a cylinder or a cone, as assumed in a recent study [11], and has a fractal geometry that spans the space with noninteger dimensions D_f [1–4]. The total length L_t of all branches inside a circle of radius t from the center of the two-dimensional discharged pattern scales in the form $L_t \sim t^{D_f}$ [2]. Thus, $n_t \sim dL_t/dt \sim t^{D_f-1}$ and $\rho_t \sim n_t/2\pi t \sim t^{D_f-2}$, where n_t is the number of branches and ρ_t is the density of the branches at a given distance t from the center. Analogous to the two-dimensional case, the three-dimensional discharged pattern is also a fractal, and it shows scaling behaviors identical to those of the two-dimensional case, except for the density $\rho_t \sim n_t/t^2 \sim t^{D_f-3}$, since the cross section is proportional to the square of the distance in three dimensions.

Now, we consider the three-dimensional conducting filament as shown in Fig. 2(a), which is a schematic illustration of three-dimensional effective conducting paths created via a dielectric breakdown; the paths extend from the top surface to the bottom surface of the insulating medium. They have treelike structures. We note that even though there exist horizontal bonds connecting branches within actual percolating paths, the current flowing across them is too small to contribute to the second and fourth moments of the current distribution. Thus, it appears to be reasonable to consider the conducting paths as effective branching trees. Now, we slice up the medium horizontally by considering a unit lattice constant Δt as shown in Figs. 2(a) and 2(b), where t is the depth or slice index from the top, n_t is the number of conducting branch segments passing through the slice t, and s_t is the lateral size of the spot area in slice t. With these definitions, we can define

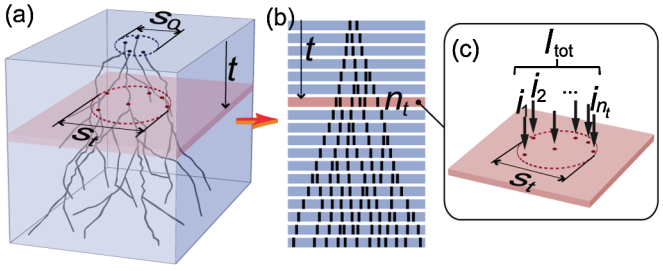

FIG. 2 (color online). (a) Branching tree structure of conducting paths generated by a dielectric breakdown; the paths extend from the top to the bottom. At the cross section at depth t, conducting spots are distributed in a region with lateral size s_t. (b) Slice structure of an insulating medium with thickness Δt. There are n_t conducting branch segments in slice t. (c) Total current I_{tot} distributed among all branch segments in a slice.

the branch segment density at slice t as $\rho_t \sim n_t/s_t^2$. The experimental fact [6,7] that multiple conducting states are generally observed during the filament rupturing process strongly implies the existence of more than one path in a bottleneck, which is located at $t = 0$ in our model, of a conducting filament. Therefore, n_t must be nonzero at $t = 0$. On the basis of this fact, we rewrite the scaling relations of n_t and ρ_t for the three-dimensional conducting paths as $n_t \sim (c_0 + t)^{D_f-1}$ and $\rho_t \sim (c_0 + t)^{D_f-3}$, where c_0 is positive; c_0 is introduced to make n_0 nonzero at $t = 0$. Note that $c_0 \sim \sqrt{n_0/\rho_0} \sim s_0$, where s_0 is the lateral dimension of the bottleneck. Therefore, we can use s_0 instead of c_0 for the derivation of scaling relations. Thus, we obtain $n_t \sim (s_0 + t)^{D_f-1}$ and $\rho_t \sim (s_0 + t)^{D_f-3}$.

Next, we consider two theoretical quantities, the second (M_2) and the fourth (M_4) moments of the current distribution. They are related to the experimentally measurable quantities, resistance of the filament R_0 [15] and the third harmonic generation signal B_{3f} [16,17], respectively, as

$$R_0 = \mathcal{R}M_2 = \mathcal{R}\sum_k \left(\frac{i_k}{I_{tot}}\right)^2, \tag{1}$$

$$B_{3f} = \mathcal{B}M_4 = \mathcal{B}\sum_k \left(\frac{i_k}{I_{tot}}\right)^4, \tag{2}$$

where the index k denotes the conducting bond, I_{tot} is the total current passing through the entire network, and $\mathcal{R}$ and $\mathcal{B}$ are the material-dependent coefficients. Then M_2 and M_4 are theoretically measurable quantities related to the geometry of the conducting paths. To calculate these moments, we approximate the current of each bond of n_t branches [18] in slice t as [Fig. 2(c)] $i_1 \approx i_2 \approx \cdots \approx i_{n_t} \approx I_{tot}/n_t$. M_2, or the resistance, is then given by

$$R_0 \propto \sum_{t=0} \left(\frac{1}{n_t}\right)^2 n_t = \sum_{t=0} \frac{1}{(s_0 + t)^{D_f-1}}.$$

The upper and lower limits for the summation above are $\int_0^N dt/(s_0 + t)^{\mathcal{D}} < R_0 < \int_0^N dt/(s_0 + t)^{\mathcal{D}} + 1/s_0^{\mathcal{D}}$, where $\mathcal{D} = D_f - 1$. If s_0 is sufficiently large so that $1/s_0^{\mathcal{D}}$ can be ignored, then $R_0 \sim \int dt/(s_0 + t)^{\mathcal{D}} \sim 1/s_0^{\mathcal{D}-1}$. Here we note that for this integration, we need the condition $D_f > 2$, which is fulfilled by the D_f value later. However, if s_0 is very small, the first term of the summation becomes dominant, so $R_0 \sim 1/s_0^{\mathcal{D}}$. In short,

$$R_0 \sim \begin{cases} s_0^{-D_f+1} & \text{for small } s_0 \\ s_0^{-D_f+2} & \text{for large } s_0. \end{cases} \tag{3}$$

In the same manner, we obtain M_4 or B_{3f}:

$$B_{3f} \propto \sum_{t=0} \left(\frac{1}{n_t}\right)^4 n_t \sim \begin{cases} s_0^{-3D_f+3} & \text{for small } s_0 \\ s_0^{-3D_f+4} & \text{for large } s_0. \end{cases} \tag{4}$$

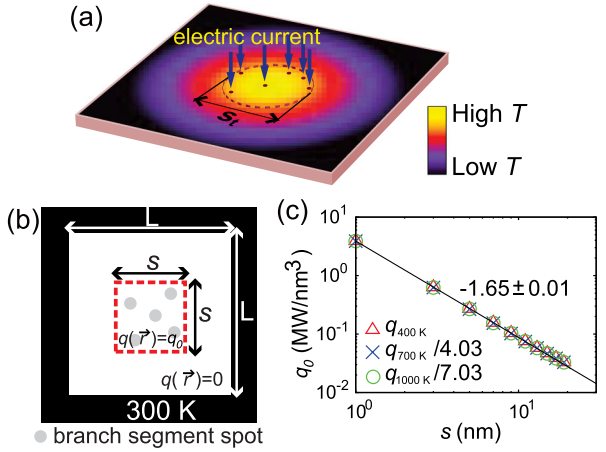

FIG. 3 (color online). (a) Electric current flowing through conducting spots (branch segments) in each slice causes Joule heating, which gives rise to a temperature gradient according to Eq. (5). When the temperature of the hottest (central) part of the slice reaches T_c [see Fig. 1(e)], rupturing occurs. (b) In simulations, we used an $L \times L$ lattice whose four boundaries were in contact with a thermal bath at temperature $T_b = 300$ K. $q(\vec{r}) = q_0$ (constant) inside the dashed (red) box with sides of length s, and $q(\vec{r}) = 0$ elsewhere. (c) FEM simulation result. We found $q_0 \sim s^{-\beta}$, with $\beta \approx 1.65 \pm 0.01$; the exponent is independent of T_c (400 K, 700 K, and 1000 K).

We introduce one more quantity, the rupture current I_R; this is the maximum current right before the rupture occurs. The rupture takes place at the hottest bond, which is located at the bottleneck in the slice $t = 0$ in Fig. 2(a). If we define i_R as the threshold current required to raise the temperature of the hottest bond up to T_c to break the bond, I_R is given by $I_R \approx i_R n_0 \sim i_R s_0^{D_f - 1}$.

Now, we explicitly take into account the manner in which the shape of the conducting paths can affect the Joule heating and rupturing process or i_R; this is achieved by using the finite element method (FEM) for simulations. As shown in Fig. 3(a), the flow of an electric current gives rise to a temperature gradient $T(\vec{r})$ according to the heat equation

$$\rho C_p \frac{dT(\vec{r})}{dt} = k\nabla^2 T(\vec{r}) + q(\vec{r}), \tag{5}$$

where ρ, C_p, k, and $q(\vec{r})$ are the density, specific heat, thermal conductivity, and heat power density, respectively, resulting from the flow of the current. Therefore, $T(\vec{r})$ is determined by $q(\vec{r})$ at a position $\vec{r}$. Now we suppose, as shown in Fig. 3(b), that branch segment spots are homogeneously distributed in an area $s \times s$ in an $L \times L$ slice so that we can approximate $q(\vec{r}) = \text{const}$, denoted as q_0, within the region $s \times s$ and consider $q(\vec{r}) = 0$ elsewhere. Here, the four boundaries are maintained at a fixed temperature of $T_b = 300$ K. We consider $L = 101$ and a unit lattice length of 1 nm. Other constituent parameters are the same as those used in Ref. [13]. In this simulation, we found the minimum q_0 that raises the temperature of the hottest (central) site of the slice up to T_c, which is the threshold temperature for on $\rightarrow$ off switching, to be a function of s. As shown in Fig. 3(c), using the FEM, we found that $q_0 \sim s^{-\beta}$, with $\beta = 1.65 \pm 0.01$, which is independent of T_c. Since the total heat generated from the branch segments in the bottleneck slice, $n_0 i_R^2 r$, is the same as the heat produced in the $s_0 \times s_0$ area, $s_0^2 q_0$, we obtain

$$i_R = \sqrt{\frac{s_0^2 q_0}{n_0 r}} = \mathcal{I} s_0^{(3-\beta-D_f)/2}, \tag{6}$$

where $\mathcal{I}$ is a material-dependent coefficient. From Eqs. (3), (4), and (6), and since $I_R \approx i_R n_0$, we can obtain the scaling relations listed in Table I.

To validate these theoretical predictions experimentally, we grew polycrystalline NiO_w, $SrTiO_x$, FeO_y, and TiO_z thin films (insulating media) on $Pt/TiO_2/SiO_2/Si$ substrates using dc magnetron reactive sputtering, pulsed laser deposition, thermal oxidation, and pulsed laser deposition, respectively. In order to determine the electrical properties, we evaporated top electrodes of 40-nm-thick Pt. We applied high voltage to the films to cause a (soft) dielectric breakdown so that conducting percolating paths could be created within them. For these films, we obtained the scaling relations between B_{3f}, R_0, and I_R. From the analysis of these scaling plots we found two scaling behaviors and their crossover values $B_{3f(\text{cross})}$, $R_{0(\text{cross})}$, and $I_{R(\text{cross})}$ for each material. To get rid of material-dependent terms and confirm the universal exponents, we used normalized quantities $B_x \equiv B_{3f}/B_{3f(\text{cross})}$, $R_x \equiv R_0/R_{0(\text{cross})}$, and $I_x \equiv I_R/I_{R(\text{cross})}$.

Figure 4(a) shows the experimental plots of B_x against R_x for the four kinds of films. The scaling relation $B_x \sim R_x^{\lambda}$ is observed in each scaling regime, and the scaling exponents seem to be universal, regardless of the oxide

TABLE I. Exponents λ, γ, and η for low and high resistance regimes. Here, we use $D_f = 2.54$ and $\beta = 1.65$ as the theoretical values.

	$B_{3f} \sim R_0^{\lambda}$		$I_R \sim R_0^{-\gamma}$		$I_R \sim B_{3f}^{-\eta}$	
	λ_l	λ_h	γ_l	γ_h	η_l	η_h
Theoretical formula with thermal effect	$\frac{3D_f-4}{D_f-2}$	3	$\frac{D_f-\beta+1}{2(D_f-2)}$	$\frac{D_f-\beta+1}{2(D_f-1)}$	$\frac{D_f-\beta+1}{2(3D_f-4)}$	$\frac{D_f-\beta+1}{6(D_f-1)}$
Theoretical values	6.7	3	1.8	0.61	0.26	0.20
Experimental values	6.7 ± 0.3	3.1 ± 0.2	1.8 ± 0.2	0.7 ± 0.1	0.24 ± 0.1	0.24 ± 0.1

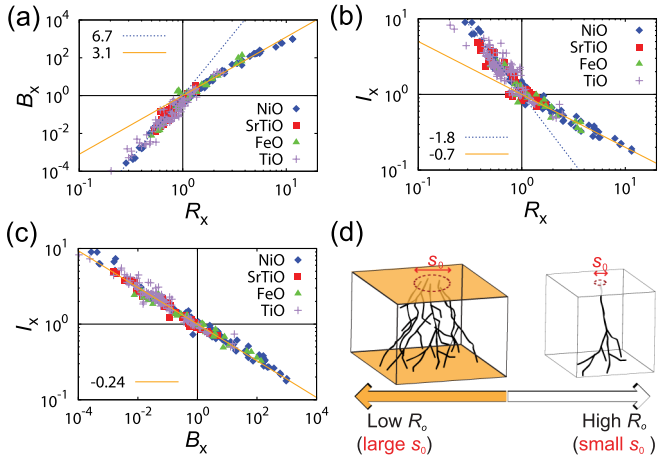

FIG. 4 (color online). (a), (b), and (c) show scaling relations for B_x vs R_x, I_x vs R_x, and I_x vs B_x, respectively. In each panel, NiO_w, $SrTiO_x$, FeO_y, and TiO_z are denoted by ◆, ■, ▲, and +, respectively. The data for NiO_w are obtained from Ref. [13]. The two scaling regions are distinguished by the $x = 10^0$ line. (d) The two scaling regions originate from different bottleneck sizes s_0 of the filaments.

materials. The exponents for the low and high resistance regimes are $\lambda_l = 6.7 \pm 0.3$ and $\lambda_h = 3.1 \pm 0.1$, respectively. Experimental plots of I_x against R_x are shown in Fig. 4(b); this figure also presents material-independent scaling behaviors corresponding to the relation $I_x \sim R_x^{-\gamma}$ in each scaling regime. The exponents for the two regimes are $\gamma_l = 1.8 \pm 0.2$ and $\gamma_h = 0.7 \pm 0.1$. We also obtained material-independent scaling exponents for the relation $I_x \sim B_x^{-\eta}$, as shown in Fig. 4(c), where $\eta_h \approx \eta_l = 0.24 \pm 0.1$; interestingly, they seem to be practically indistinguishable. These experimentally measured exponent values are in excellent agreement with the theoretical values when we choose $D_f = 2.54$. Actually, this D_f value was chosen to make the theoretical value match the experimental value of λ_l, but is in good agreement with a previous simulation result in the range 2.32–2.65 [19] for a three-dimensional diffusion limited aggregation pattern, which is known to share a common fractal nature with the dielectric breakdown pattern [1].

This study has clarified the physical meaning of the two scaling regimes. They are separated by the number of bottleneck links of percolating paths, as depicted in Fig. 4(d). The bottleneck on the percolating paths consists of many connections with large s_0 for low resistance values and very few connections with small s_0 for high resistance values. The universal behaviors indicate that the topology of the conducting path is preserved for different materials, which is of crucial importance not only in scientific research, as a topic of wide interest, but also in engineering; we can adapt the same technique to devices composed of different materials.

Finally, we remark that the two scaling regimes are formed in a self-organized manner during the switching dynamics, which comprise the dielectric breakdown and thermal rupture processes. This differs from the formation mechanism of the two scaling regimes in the conventional percolation, in which the bottleneck size is comparable to the correlation length determined from the fraction of conducting bonds.

This research was supported by the National Research Foundation of Korea Grants No. 2010-0015066 (B. K.), No. 2009-0080567 (T. W. N.), No. 2010-0020416 (T. W. N.), and No. 2010-0011608 (B. S. K.), and by the NAP of KRCF (B. K.).

*twnoh@snu.ac.kr
†bkahng@snu.ac.kr

[1] L. M. Sander, Nature (London) **322**, 789 (1986).
[2] L. Niemeyer, L. Pietronero, and H. J. Wiesmann, Phys. Rev. Lett. **52**, 1033 (1984).
[3] H. Takayasu, Phys. Rev. Lett. **54**, 1099 (1985).
[4] D. ben-Avraham and S. Havlin, *Diffusion and Reactions in Fractal and Disordered Systems* (Cambridge University Press, Cambridge, England, 2000).
[5] R. Waser *et al.*, Adv. Mater. **21**, 2632 (2009).
[6] M.-J. Lee *et al.*, Nano Lett. **9**, 1476 (2009).
[7] S.-E. Ahn *et al.*, Adv. Mater. **20**, 924 (2008).
[8] S. C. Chae *et al.*, Adv. Mater. **20**, 1154 (2008).
[9] U. Russo *et al.*, IEEE Trans. Electron Devices **56**, 193 (2009).
[10] R. Waser and M. Aono, Nature Mater. **6**, 833 (2007).
[11] D.-H. Kwon *et al.*, Nature Nanotech. **5**, 148 (2010).
[12] S. H. Chang *et al.*, Phys. Rev. Lett. **102**, 026801 (2009).
[13] S. H. Chang *et al.*, Appl. Phys. Lett. **92**, 183507 (2008).
[14] L. de Arcangelis and H. J. Herrmann, Phys. Rev. B **39**, 2678 (1989).
[15] S. B. Lee *et al.*, Appl. Phys. Lett. **93**, 212105 (2008).
[16] M. A. Dubson *et al.*, Phys. Rev. B **39**, 6807 (1989).
[17] Y. Yagil, G. Deutscher, and D. J. Bergman, Phys. Rev. Lett. **69**, 1423 (1992).
[18] B. Kahng, G. G. Batrouni, and S. Redner, J. Phys. A **20**, L827 (1987).
[19] P. Meakin, Phys. Rev. A **27**, 1495 (1983).